Journal of Zhejiang University-SCIENCE A (Applied Physics & Engineering)
ISSN 1673-565X (Print); ISSN 1862-1775 (Online)
www.jzus.zju.edu.cn; www.springerlink.com
E-mail: jzus@zju.edu.cn

Simulation and experimental evaluation of a combustion-powered actuator for hopping*

Yun-guang LUAN[1,3], Hua-ming WANG[†‡1,2], Dong-biao ZHAO[1], Yang WANG[1], Feng-hong CHEN[1]

([1]*College of Mechanical and Electronical Engineering, Nanjing University of Aeronautics and Astronautics, Nanjing 210016, China*)

([2]*State Key State Key Laboratory of Fluid Power and Mechatronic Systems, Zhejiang University, Hangzhou 310027, China*)

([3]*Department of Mechatronics, Suzhou Vocational Institute of Industrial Technology, Suzhou 215104, China*)

[†]E-mail: hmwang@nuaa.edu.cn

Received Dec. 9, 2016; Revision accepted Mar. 21, 2017; Crosschecked Sept. 19, 2017

Abstract: A combustion-powered actuator has been proposed in our previous work (Wang *et al*., 2015), and it has shown great power hopping ability. To explore the hopping process and output performance of the actuator, the model of an actuator driving the hopping process is investigated through theoretical analysis and experimental validation. Firstly, the structure of the actuator and hopping process are described briefly, and the dynamic models of the process are constructed. Secondly, the thermodynamic model of the actuator is established by the Wiebe heat release function and the input energy density is computed by Chemkin for when propane and nitrous oxide with different equivalence ratios are injected into the chamber. Thus, the thermodynamic model is obtained by integrating dynamic and thermodynamic equations. After that, a few output performance parameters are identified to assess system performance. Lastly, the experimental rig of the combustion actuator is set up to test the displacement and pressure of the actuator driven hopping process. By solving the thermodynamic equations, the post-combustion pressure, the displacement and the velocity varying with time are computed, and are compared with the test results, indicating that the computational results match the experimental test well. At the end of the stroke, the velocities of the experiment and simulation are 6.5 m/s and 6.99 m/s, respectively. The hopping results are compared with the simulation when different pressures under equivalence ratio of 1 are injected, and the maximum and minimum deviations are 14.45% and 1.83%, respectively.

Key words: Thermodynamic model; Combustion-powered actuator; Simulation analysis; Experimental analysis; Output performance

http://dx.doi.org/10.1631/jzus.A1600773 **CLC number:** TP242

1 Introduction

Hopping robots can travel across obstacles several times their body size (Kovac *et al*., 2008). However, the robots need proper actuators to deliver very large power while driving the hopping process. Conventional hopping actuators (electrical motors) mostly depend on energy accumulation and impulsive energy trigger mechanisms to meet this output requirement (Burdick and Fiorini, 2003; Nguyen and Park, 2012; Zhao *et al*., 2013). However, combustion-powered actuators do not need these mechanisms because of their large power merit, which brings the advantages of lighter mass and higher energy efficiency. Additionally, the actuators have the merit of high energy density for their energy coming from fossil fuels (Rakopoulos *et al*., 2011). Therefore, they are especially suitable for field robots moving on unknown terrain with large obstacles.

Combustion-powered devices have been widely applied in many fields such as automation (Mikalsen and Roskilly, 2007), compressors (Fite and Goldfarb, 2006; Willhite *et al*., 2013), generators (Li *et al*.,

‡ Corresponding author

* Project supported by the Innovation Foundation of the State Key State Key Laboratory of Fluid Power and Mechatronic Systems (No. GZKF-201406), Zhejiang University, China

ORCID: Yun-guang LUAN, http://orcid.org/0000-0002-0632-6381

2008; Jia *et al*., 2015), and hydraulic pumps (Stergiopulos *et al*., 2014). However, actuators with combustion were first used to power a hopping robot just after the year 2000. The idea was initiated by the Sandia State Laboratory, USA and relevant patents were proposed (Spletzer *et al*., 2001). Then, a four-wheel robot with the combustion-powered actuator was designed (Fischer, 2005). After that, the hopping robot Sandflea, which was improved by the Boston Dynamic Laboratory, USA, could hop 1 m to 8 m high (Ackerman, 2012). Wang *et al.* (2012) proposed a combustion-powered actuator and investigated the performance of the actuator by experiment, and the results showed that the actuator has a better payload ability than other methods such as electrical motors and dielectric elastomer actuators (Wang *et al*., 2015). Luan *et al*. (2015) studied the influence of different mixing ratios between propane and nitrous oxide and initial injection pressures on the hopping height by experiments and analyzed the effect of different force behaviors of grounds on the performance of combustion-powered hopping robots (Luan *et al*., 2016). Recently, combustion actuation was used to drive soft robots. For example, Tolley *et al.* (2014) presented an untethered robot that can jump 0.6 m (7.5 times of its body height) vertically and 0.6 m laterally using pneumatic and explosive actuators. Loepfe *et al.* (2015) developed a roly-poly geometry soft jumping robot powered by nitrous oxide and propane.

Although hopping robots with combustion actuation have been studied for a long time, most attention has been focused on the mechanical structures of actuators and robots. Research on the thermodynamics of the combustion actuator is limited. The main reason is that the working process of the actuator is influenced by many factors such as injection pressure, equivalence ratio, spark position, and chamber structures, with the result that the combustion-powered hopping robot is very difficult to control. To analyze the performance of the actuator and control the hopping height, the thermodynamic model should be studied. Many theoretical methods have been used to study the thermodynamic model of combustion-powered actuations in other applications to analyze and control their driving process (Mikalsen and Roskilly, 2009; Kim *et al*., 2013). The current paper explores the thermodynamic model and output performance of our actuator by numerical and experimental methods.

2 Structure and working principle of the actuator

The schematic diagram of the actuator, including its gas injection system, is shown in Fig. 1. The actuator, which mainly consists of a cylinder-piston assembly, whose piston is designed as a double-piston structure, is similar to spark ignition linear free piston engines (Li *et al*., 2009). However, there are some differences between them:

1. The cylinder of the actuator is free and is used to do external work, while the piston pushes against ground.

2. The actuator does not have intake and compression strokes and depends on solenoid valves to control the gas injection and exhaust.

3. The actuator can endure more misfires than free piston engines as it works in intermittence mode, while most free piston engines work on continuous mode. Once the ignition fails, the source gases can be injected and re-sparked again.

The structural specifics of the actuator are shown in Table 1.

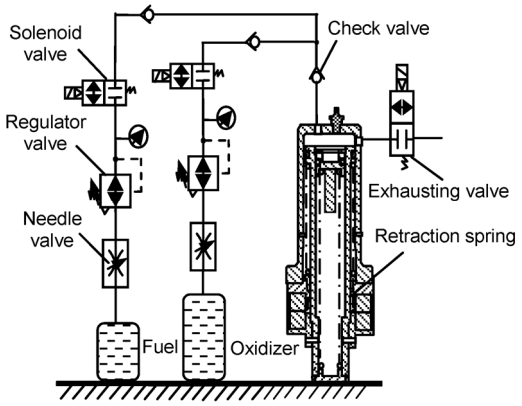

Fig. 1 Schematic diagram of the actuator including an injection system

Table 1 Specifics of the actuator

Parameter	Value
Diameter of cylinder bore (mm)	37
Length of stroke (mm)	48
Mass of cylinder and its accessories (g)	390
Mass of piston and its accessories (g)	350

Conventional internal engines mostly use liquid fuels, such as gasoline and diesel, as energy sources. These fuels have the merits of excellent energy-volume ratio, high energy-mass ratio, and easy storage. However, these fuels need complex carbureting devices to inject into the chamber, which will add more weight to the actuator and reduce its energy efficiency. To simplify the injection system, gas fuel sources propane (99.9%) and nitrous oxide (>99%) are selected as fuel and oxidizer, respectively, both of which have a self-pressurization property (Tiliakos *et al*., 2001) and can be easily controlled by solenoid valves.

During the working process, the actuator goes through the following three stages:

(1) Gas injection

The propane is injected first, because its injection pressure is lower than that of nitrous oxide. When the propane is injected, the valves of the nitrous oxide circuit are closed and all valves of the propane circuit are open. When nitrous oxide is injected, the opposite operation is conducted.

(2) Combustion and expansion

When the injection is finished, all valves are closed for spark. When the igniter sparks the gas mixture inside the chamber, the chemical energy is released immediately. The cylinder, which is under the pressure of the post-combustion gases, begins to accelerate upward and the volume of the chamber increases.

(3) Exhaust

After the combustion and expansion stage ends, the exhaust valve is open, and the pressure drops to atmospheric pressure. The piston is returned by the retraction spring, and then the remaining gas is discharged.

3 Thermodynamic model of driving hopping

The combustion-powered hopping process, as illustrated in Fig. 2, includes driving, collision, and flight.

3.1 Dynamic model

Because the cylinder is free, its motion is determined by the forces on it. During the driving stage, the forces that act on the cylinder and piston are illustrated in Fig. 3. Assuming the piston pushes against hard ground, the piston will keep still at the equilibrium force state due to the reaction force of ground F_N. According to Newton's second law, the dynamic equation of the cylinder is derived as

$$m_1\ddot{s} = (p - p_0)A - m_1 g - f - k(l_0 + s) - F_M - c\dot{s}, \quad (1)$$

where m_1 is the total mass of cylinder, its accessories, and the payload, s is the displacement of the cylinder, p is the pressure inside the chamber, p_0 is the environmental pressure, A is the area of the cylinder bore, f is the friction force between the cylinder and the piston, k and l_0 are the stiffness and initial length of the retraction spring, respectively, F_M is the magnetic latch force, and c is the damped coefficient, as estimated by (Tsukagoshi *et al*., 2005)

$$c = 50 \times 2\sqrt{A\pi}. \quad (2)$$

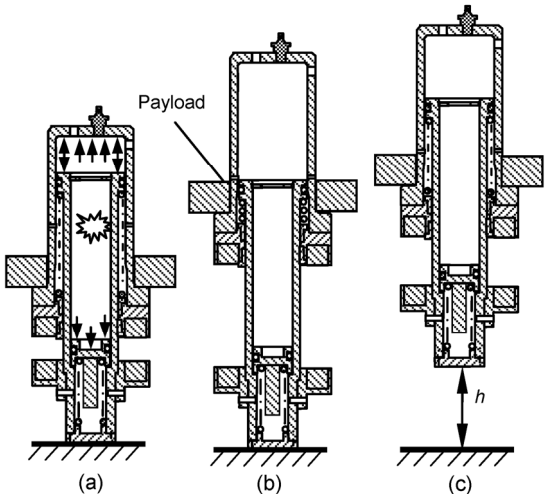

Fig. 2 Schematic view of actuator driving hopping process: (a) driving, (b) collision, and (c) flight
Arrows in Fig. 2a mean pressures of the post-combustion gases

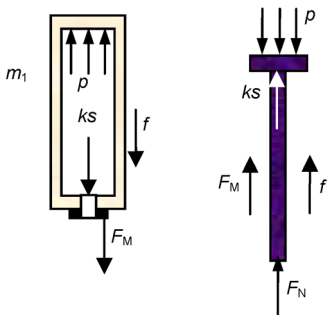

Fig. 3 Forces applied on cylinder and piston

To make the system first order, the velocity of the cylinder v is introduced. Then, Eq. (1) can be changed to:

$$\begin{cases}\dot{s}=v,\\ \dot{v}=[(p-p_0)A-m_1g-f-k(l_0+s)-F_{\mathrm{M}}-cv]/m_1.\end{cases} \tag{3}$$

If the force of the pressure inside the chamber is smaller than the resultant of the other forces at the initial time, the cylinder will keep still. The equations are changed as

$$\begin{cases}\dot{s}=0,\\ \dot{v}=0,\end{cases} \text{ if } (p-p_0)A\le m_1g+f+k(l_0+s)+F_{\mathrm{M}}. \tag{4}$$

To obtain the magnetic latch force, a test device shown in Fig. 4 is established. The cylinder is fixed to a bracket, and the piston is fastened to a force sensor with a moving table via a socket. Thus, the magnetic latch force-displacement curve can be acquired as shown in Fig. 5.

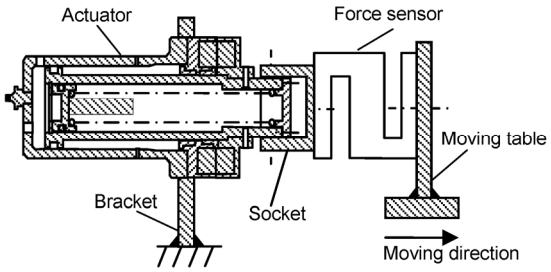

Fig. 4 Schematic diagram of force test setup

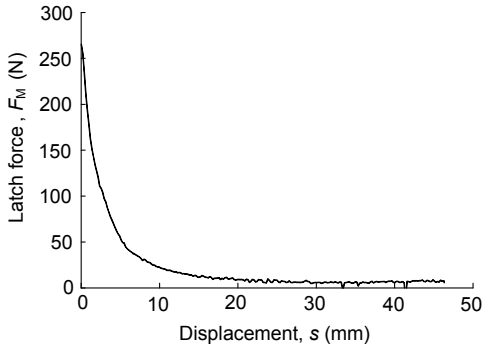

Fig. 5 Magnetic latch force-displacement relationship

The formula of the latch force-displacement can be fitted as

$$F_{\mathrm{M}}(s)=1.1+\frac{258.9}{1+\left(\dfrac{s}{1.86899}\right)^{1.39296}}. \tag{5}$$

Referring to (Tsukagoshi *et al*., 2005), the friction force is given as

$$f=330\times 2\sqrt{A\pi}. \tag{6}$$

When the displacement of the cylinder moves to the stroke position, the cylinder will collide with the piston and they will hop at the same velocity. According to the momentum conservation law, the velocity after collision can be obtained:

$$v_2=\frac{m_1v_1}{m_1+m_2}, \tag{7}$$

where v_1 is the velocity of the cylinder before collision, and m_2 is the total mass of piston and its accessories.

By conservation of energy, neglecting the air resistance, the hopping height h is derived from:

$$h=\frac{m_1^2v_1^2}{2(m_1+m_2)^2g}. \tag{8}$$

3.2 Thermodynamic model

The schematic of the pressure change inside the chamber is shown in Fig. 6. During the injection period, the pressure gradually increases from atmosphere pressure to a set pressure. After sparking, the actuator carries on the combustion and expansion period and the pressure immediately increases. When the pressure is up to the maximum pressure, it will decrease due to the expansion of the volume. After the cylinder is up to the stroke position, the pressure will drop to atmospheric pressure because the exhaust solenoid valve is open. Before thermodynamic modeling, the following assumptions are needed:

(1) The gas inside the chamber is an ideal gas.

(2) There is no leak during the actuation process.

According to the first law of thermodynamics, the following equation can be given by

$$\frac{\mathrm{d}Q}{\mathrm{d}t}=\frac{\mathrm{d}U}{\mathrm{d}t}+\frac{\mathrm{d}W}{\mathrm{d}t}+\frac{\mathrm{d}Q_\mathrm{s}}{\mathrm{d}t}, \tag{9}$$

where Q is the released heat, U is the internal energy of the gas, W is the work that the gas inside the chamber has done, and Q_s is the heat transferred by the wall.

The differential form of the state equation is defined by

$$p\frac{\mathrm{d}V}{\mathrm{d}t}+V\frac{\mathrm{d}p}{\mathrm{d}t}=R_\mathrm{m}T\frac{\mathrm{d}m}{\mathrm{d}t}+mR_\mathrm{m}\frac{\mathrm{d}T}{\mathrm{d}t}, \tag{10}$$

where V is the volume of the chamber, R_m is the gas constant, m is the mass of the gas, and T is the temperature of the gas.

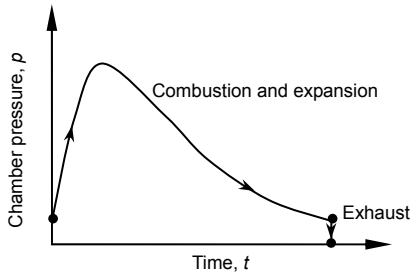

Fig. 6 Schematic diagram of pressure change with time

The internal energy change is

$$\frac{\mathrm{d}U}{\mathrm{d}t}=\bar{c}_\mathrm{V}m\frac{\mathrm{d}T}{\mathrm{d}t}+\bar{c}_\mathrm{V}T\frac{\mathrm{d}m}{\mathrm{d}t}, \tag{11}$$

where $\bar{c}_\mathrm{V}$ is the average heat capacity of the gas. For a closed system, dm/dt=0.

The rate of work is given by

$$\frac{\mathrm{d}W}{\mathrm{d}t}=p\frac{\mathrm{d}V}{\mathrm{d}t}. \tag{12}$$

Substituting Eqs. (10)–(12) into Eq. (9) gives:

$$\frac{\mathrm{d}Q}{\mathrm{d}t}=\left(\frac{\bar{c}_\mathrm{V}}{R_\mathrm{m}}\right)V\frac{\mathrm{d}p}{\mathrm{d}t}+\left(\frac{\bar{c}_\mathrm{V}}{R_\mathrm{m}}+1\right)p\frac{\mathrm{d}V}{\mathrm{d}t}+\frac{\mathrm{d}Q_\mathrm{s}}{\mathrm{d}t}. \tag{13}$$

The pressure and temperature are obtained from Eqs. (9)–(13):

$$\frac{\mathrm{d}p}{\mathrm{d}t}=\frac{1}{V}\left[(\gamma-1)\left(\frac{\mathrm{d}Q}{\mathrm{d}t}-\frac{\mathrm{d}Q_\mathrm{s}}{\mathrm{d}t}\right)-p\gamma\frac{\mathrm{d}V}{\mathrm{d}t}\right], \tag{14}$$

$$\frac{\mathrm{d}T}{\mathrm{d}t}=\frac{1}{m\bar{c}_\mathrm{V}}\left(\frac{\mathrm{d}Q}{\mathrm{d}t}-\frac{\mathrm{d}Q_\mathrm{s}}{\mathrm{d}t}-p\frac{\mathrm{d}V}{\mathrm{d}t}\right), \tag{15}$$

where γ is the specific heat capacity. The following relation exists:

$$R_\mathrm{m}/\bar{c}_\mathrm{V}=\gamma-1. \tag{16}$$

The average heat capacity is calculated by

$$\bar{c}_\mathrm{V}=\sum_{n_i}^{n_\mathrm{t}}n_ic_{\mathrm{V}i}, \tag{17}$$

where n_i is the mass concentration coefficient of species i, n_t is the total number of the species of the combustion gas, and $c_{\mathrm{V}i}$ is the heat capability of species i.

According to the Arrehnius law, the Wiebe function is used to describe the combustion model. The combustion fraction of the gas is given by

$$\chi=1-\exp\left[-6.908\left(\frac{t-t_\mathrm{s}}{t_\mathrm{d}}\right)^{n+1}\right], \tag{18}$$

where t_s is the time that combustion occurs, t_d is the combustion duration, and n is the combustion quality factor (about 1–3) (Ghojel, 2010).

Then the heat release change can be given by

$$\frac{\mathrm{d}Q}{\mathrm{d}t}=E_\mathrm{m}m_\mathrm{g}\eta\frac{\mathrm{d}\chi}{\mathrm{d}t}, \tag{19}$$

where E_m is the energy density of the gas, m_g is the mass of the gas, and η is the combustion efficiency. Because the start combustion time is considered as zero, t_s equals 0. Substituting Eq. (18) into Eq. (19), the equation is changed to:

$$\begin{aligned}\frac{\mathrm{d}Q}{\mathrm{d}t}=&H_\mathrm{m}m\eta 6.908\frac{n+1}{t_\mathrm{d}}\left(\frac{t}{t_\mathrm{d}}\right)^n\\&\cdot\exp\left[-6.908\left(\frac{t}{t_\mathrm{d}}\right)^{n+1}\right],\end{aligned} \tag{20}$$

where H_m is the reaction enthalpy.

The heat transfer rate is governed by

$$\frac{\delta Q_s}{\delta t}=\alpha_s A'(T-T_w), \tag{21}$$

where T_w is the temperature of the cylinder and piston wall, and it equals the environmental temperature 300 K. α_s and A' are the heat transfer coefficient and the area of the transfer heat wall, respectively.

To calculate the heat transfer coefficient, the expression is given by (Tsukagoshi *et al*., 2005)

$$\alpha_s=50\times 2s\sqrt{A\pi}. \tag{22}$$

The transfer heat wall, including cylinder top, piston top, cylinder side and piston side walls, is expressed as

$$A'=\frac{\pi D^2}{4}+\pi Ds+\pi dl+\frac{\pi d^2}{4}, \tag{23}$$

where D and d are the cylinder bore and piston bore, respectively, and l is the length of the piston cavity.

The volume change is given by

$$\frac{\mathrm{d}V}{\mathrm{d}t}=A_p\frac{\mathrm{d}s}{\mathrm{d}t}, \tag{24}$$

where A_p is the area of the cylinder bore.

Substituting Eqs. (20)–(24) into Eqs. (14) and (15), the equations of the thermodynamic model can be obtained. Combining the thermodynamic equations with the dynamic Eqs. (3) and (4), the thermodynamic equations are obtained.

If $(p-p_0)A\le m_1 g+f+k(l_0+s)+F_M$,

$$\begin{cases}\dfrac{\mathrm{d}p}{\mathrm{d}t}=\dfrac{1}{V}\left[(\gamma-1)\left(\dfrac{\mathrm{d}Q}{\mathrm{d}t}-\dfrac{\mathrm{d}Q_s}{\mathrm{d}t}\right)-p\gamma\dfrac{\mathrm{d}V}{\mathrm{d}t}\right],\\ \dfrac{\mathrm{d}T}{\mathrm{d}t}=\dfrac{1}{m\bar{c}_V}\left(\dfrac{\mathrm{d}Q}{\mathrm{d}t}-\dfrac{\mathrm{d}Q_s}{\mathrm{d}t}-p\dfrac{\mathrm{d}V}{\mathrm{d}t}\right),\\ \dfrac{\mathrm{d}v}{\mathrm{d}t}=0,\\ \dfrac{\mathrm{d}V}{\mathrm{d}t}=0.\end{cases} \tag{25}$$

If $(p-p_0)A>m_1 g+f+k(l_0+s)+F_M$,

$$\begin{cases}\dfrac{\mathrm{d}p}{\mathrm{d}t}=\dfrac{1}{V}\left[(\gamma-1)\left(\dfrac{\mathrm{d}Q}{\mathrm{d}t}-\dfrac{\mathrm{d}Q_s}{\mathrm{d}t}\right)-p\gamma\dfrac{\mathrm{d}V}{\mathrm{d}t}\right],\\ \dfrac{\mathrm{d}T}{\mathrm{d}t}=\dfrac{1}{m\bar{c}_V}\left(\dfrac{\mathrm{d}Q}{\mathrm{d}t}-\dfrac{\mathrm{d}Q_s}{\mathrm{d}t}-p\dfrac{\mathrm{d}V}{\mathrm{d}t}\right),\\ \dfrac{\mathrm{d}v}{\mathrm{d}t}=\dfrac{A(p-p_0)-m_1 g-f-k(l_0+s)-F_M-cv}{m_1},\\ \dfrac{\mathrm{d}V}{\mathrm{d}t}=Av.\end{cases} \tag{26}$$

To calculate the input energy density and the specific heat capacity, Chemkin is used (Kee *et al*., 2006). The GRI-Mech 3.0 reaction mechanism is chosen, and the thermodynamic and transfer data for species are taken from Powell *et al*. (2010). The energy density varying with equivalence ratio is shown in Fig. 7. From Fig. 7, the energy density that peaks at equivalence ratio of 1 is 5905.98 J/g. The percentages of main species are shown in Table 2. The specific heat ratios of these species are obtained from the NIST-JANAF table, and then γ can be obtained according to Eqs. (16) and (17).

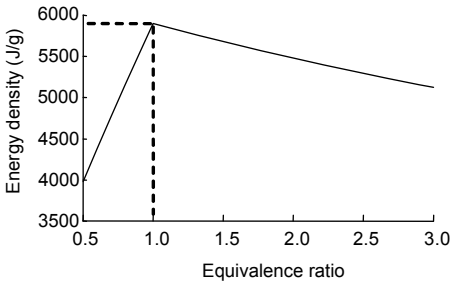

Fig. 7 Energy density varying with equivalence ratio

Table 2 Percentages of main species

Species	Percentage (%)	Species	Percentage (%)
N_2	52	NO	3.1
H_2O	16	H_2	2.8
CO	10	H	2
CO_2	6.8	O	1.4
OH	4.5		

3.3 Output performance parameters

To assess the performance of the actuator, the following parameters are identified referring to the parameters of internal engines.

Indicated work is work that the gas does via the cylinder. The expression is given by

$$W=\int_{V_0}^{V_e} p\mathrm{d}V, \tag{27}$$

where V_e is the volume when the cylinder moves up to the stroke position, and V_0 is the initial volume.

Indicated work efficiency is defined as the indicated work divided by the input energy:

$$\eta=\frac{W}{Q_{in}}=\frac{W}{H_m m_g}. \tag{28}$$

Average power is calculated as

$$P=\frac{W}{t}. \tag{29}$$

Hopping efficiency is the hopping energy divided by the input energy:

$$\eta_h=\frac{mgh}{Q_{in}}=\frac{mv_2^2}{2Q_{in}}. \tag{30}$$

4 Experiments and simulation

To validate the thermodynamic model, the measurement setup consists of a top plate, sensors, linear bearings, cushions, direction guide plates, and a data acquisition (DAQ) card, as presented in Fig. 8. The displacement of the cylinder and the pressure inside the chamber are measured by a potentiometer and a large pressure sensor, respectively. Because the quantities of propane and nitrous oxide are not easy to control directly, they are calculated by their injection pressures according to the ideal gas equation. The pressure of 0.188 MPa of nitrous oxide under equivalence ratio of 1 is used to power the hopping experiment. In our previous work, hopping experiments conducted outdoors (Luan *et al*., 2015) are used to estimate parameters such as combustion duration and combustion efficiency.

The specifications in the simulation are shown in Table 3. Substituting the parameters of Table 3 into Eqs. (27) and (28), and the initial condition of p_0= 0.288×10^{-6} Pa (absolute pressure), T_0=273.15 K, v_0= 0 m/s, V_0=0 m^3, the equations can be solved by the Runge-Kutta method.

Table 3 Specifications of simulation

Parameter	Value
Payload (kg)	2.43
Wall temperature, T_W (K)	300
Initial volume, V_0 (m^3)	9.573×10^{-6}
Combustion efficiency, η (%)	~37
Combustion duration, t_d (ms)	~5
Combustion quality factor, n	1
Specific heat ratio, γ	1.31
End volume, V_e (m^3)	38.132×10^{-6}
Mass of C_3H_8 (mg)	17.6
Mass of N_2O (mg)	176

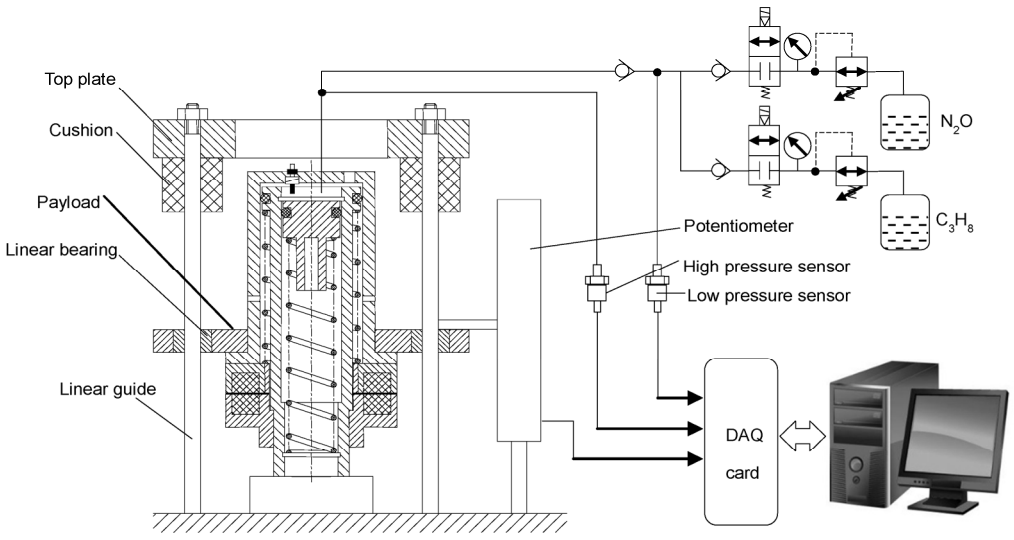

Fig. 8 Schematic view of actuator measurement plate

Between the payload and cushion, there is 120 mm of space that the mechanism can move upward, which is larger than the stroke of the actuator, to alleviate the impact force when the collision occurs between the mechanism and cushion. Therefore, the mechanism will experience driven hopping, collision between cylinder and piston, hopping in the flight, collision and landing in the experiment. The curves of the pressure, velocity, and displacement of the experiment (solid) and the simulation (dash) are shown in Fig. 9. From Fig. 9a, the total time is 100 ms from the spark time to when the mechanism lands, and when the actuator gets up to the stroke position at 48 mm, the time is 14.8 ms and in the simulation it consumes 12.6 ms. Thus, there is a 2.2 ms difference between the experiment and the simulation, and this is caused by the mounted gap between the potentiometer and the payload, and there is a little friction between the guide and the bearing, which is ignored in the simulation.

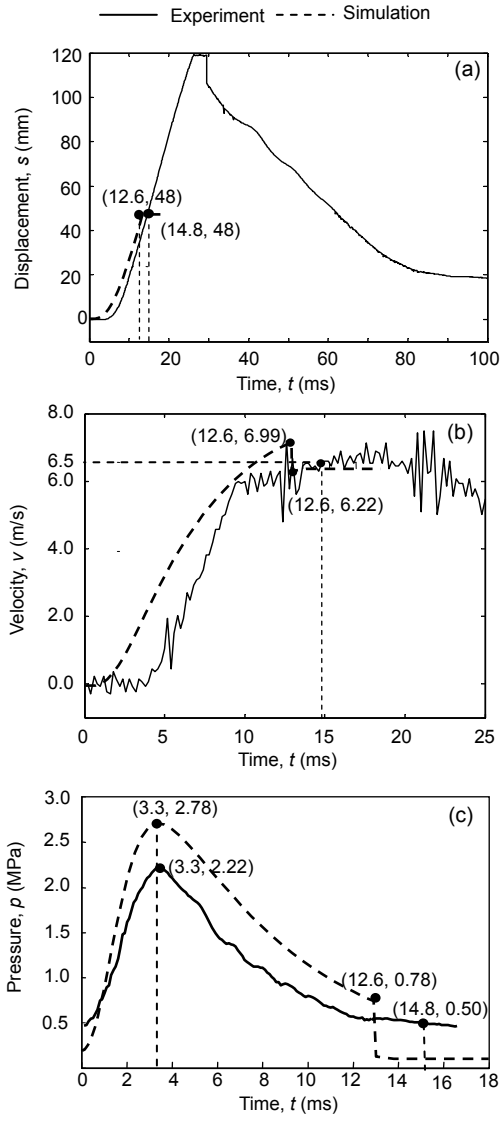

Fig. 9 Comparison of displacement (a), velocity (b), and pressure (a) between experiment and simulation

The velocity of the experiment, shown in Fig. 9b, is calculated from the measured displacement-time data. From Fig. 9b, the velocity of the experiment, when the cylinder reaches the stroke position, is 6.5 m/s, but the velocity increases further. This is because the pressure cannot decrease to atmospheric pressure instantly. Finally, the velocity after collision is 6 m/s. However, according to the simulation, the velocities, which are before and after collision, are 6.99 m/s and 6.22 m/s, respectively.

As shown in Fig. 9c, the pressure of the experiment drops to 0.5 MPa when the cylinder gets to the stroke 48 mm. It is not expected, as it is in the simulation, that the pressure falls to environmental pressure instantly. This is because the exhaust hole is not large enough. Then it still has the ability to do external work if the stroke is enlarged.

From section 3.3, the output performance parameters, according to the thermodynamic model and the experimental test, are shown in Table 4.

From Table 4, the result of the simulation deviates a little from the experiment. Thus, the simulation can be used to calculate the output performance. Table 4 shows that the power density of the actuator is 6.19 kW/kg, which is much larger than that of electric motors which is about 0.05 kW/kg.

Table 4 Performance parameters between simulation and experiment

Parameter	Value	
	Simulation	Experiment
Indicated work (J)	78.49	67.80
Indicated efficiency (%)	6.86	5.93
Average power (kW)	6.23	4.58
Hopping efficiency (%)	5.36	4.99
Power density (kW/kg)	8.42	6.19

To verify the model, experiments of different injection pressures under stoichiometric ratio are conducted. The results of simulation and experiment are shown in Table 5.

From Table 5, the maximum deviation between experiment and simulation is 14.45%. Therefore, the model can be used to calculate the hopping velocity.

Table 5 Velocities of different injection pressures -comparison between simulation and experiment

Injection pressure (MPa)	Velocity (m/s)		Deviation (%)
	Simulation	Experiment	
0.18	6.10	5.33	14.45
0.20	6.39	6.10	4.75
0.21	6.45	6.57	1.83

From the results, the actuator indicated efficiency is less than 10%, which is lower than a conventional engine at about 30%. According to a patent (Spletzer *et al*., 2001), the hopping efficiency of the combustion-powered rigid mechanism is about 15%, while a combustion-powered soft hopping robot is less than 1% (Tolley *et al*., 2014; Loepfe *et al*., 2015). From our previous experiments (Luan *et al*., 2015), the main reason that the combustion efficiency of the actuator is lower than conventional engines is that they can control the piston to improve the efficiency. Thus, how to improve the hopping efficiency is a key issue for the next step.

The hopping velocity is the key parameter because the hopping height of the robot is given by the velocity. According to Eq. (8), the height is the quadratic function of the velocity. If the velocity changes a little, the result of the height changes a lot. Thus, the model that is developed for the hopping robot can be used to analyze the height of the combustion-powered hopping robot and provide guidance for the actuator design to improve the output performance of the hopping robot. The thermodynamic model can be used to simulate the driving hopping process, but it is still necessary to determine three parameters of combustion model, namely combustion time, combustion quality, and combustion efficiency empirically. Therefore, further research is needed to investigate the combustion mechanism to obtain the parameters by the numerical method.

5 Conclusions

In this paper, we have modeled the combustion-powered hopping actuator, and investigated its output performance. The following conclusions are drawn.

1. The dynamic and thermodynamic model of the combustion-powered actuator for hopping is established. The energy density of source is determined by Chemkin when different equivalence ratio mixtures (propane and nitrous oxide) are injected.

2. An experiment on the actuator, which powers hopping, is conducted. The displacement and the pressure inside the chamber are measured. The results of the experiment are compared with the simulation. There is a good consistency between them. Finally, the output performance parameters, according to the simulation and experimental test, are calculated. There is a small deviation.

References

Ackerman, E., 2012. Boston dynamics sand flea robot demonstrates astonishing jumping skills. IEEE Spectrum Robotics Blog. http://spectrum.ieee.org/automaton/robotics/military-robots/boston-dynamics-sand-flea-demonstrates-astonishing-jumping-skills [Accessed on Mar. 28, 2016]

Burdick, J., Fiorini, P., 2003. Minimalist jumping robots for celestial exploration. *The International Journal of Robotics Research*, **22**(7-8):653-674. http://dx.doi.org/10.1177/02783649030227013

Fischer, G.J., 2005. Wheeled hopping mobility. European Symposium on Optics and Photonics for Defence and Security, No. 59860H. http://dx.doi.org/10.1117/12.634896

Fite, K.B., Goldfarb, M., 2006. Design and energetic characterization of a proportional-injector monopropellant-powered actuator. *IEEE/ASME Transactions on Mechatronics*, **11**(2):196-204. http://dx.doi.org/10.1109/TMECH.2006.871097

Ghojel, J.I., 2010. Review of the development and applications of the Wiebe function: a tribute to the contribution of Ivan Wiebe to engine research. *International Journal of Engine Research*, **11**(4):297-312. http://dx.doi.org/10.1243/14680874JER06510

Jia, B., Tian, G., Feng, H., *et al*., 2015. An experimental investigation into the starting process of free-piston engine generator. *Applied Energy*, **157**:798-804. http://dx.doi.org/10.1016/j.apenergy.2015.02.065

Kee, R.J., Rupley, F.M., Miller, J.A., *et al*., 2006. CHEMKIN Release 4.1, Reaction Design. San Diego, California, USA.

Kim, J., Bae, C., Kim, G., 2013. Simulation on the effect of the combustion parameters on the piston dynamics and engine performance using the Wiebe function in a free piston engine. *Applied Energy*, **107**:446-455. http://dx.doi.org/10.1016/j.apenergy.2013.02.056

Kovac, M., Fuchs, M., Guignard, A., *et al*., 2008. A miniature 7g jumping robot. IEEE International Conference on Robotics and Automation, p.373-378.

Li, Q.F., Xiao, J., Huang, Z., 2008. Simulation of a two-stroke

free-piston engine for electrical power generation. *Energy & Fuels*, **22**(5):3443-3449. http://dx.doi.org/10.1021/ef800217k

Li, Q.F., Xiao, J., Huang, Z., 2009. Flat-type permanent magnet linear alternator: a suitable device for a free piston linear alternator. *Journal of Zhejiang University-SCIENCE A*, **10**(3):345-352. http://dx.doi.org/10.1631/jzus.A0820224

Loepfe, M., Schumacher, C.M., Lustenberger, U.B., *et al*., 2015. An untethered, jumping roly-poly soft robot driven by combustion. *Soft Robotics*, **2**(1):33-41. http://dx.doi.org/10.1089/soro.2014.0021

Luan, Y.G., Wang, H.M., Zhao, D.B., *et al*., 2015. Analysis and experiment of combustion powered linear actuator for hopping. *Robot*, **37**(4):499-505 (in Chinese).

Luan, Y.G., Wang, H.M., Zhao, D.B., *et al*., 2016. Hopping ability of gas fuel power hopping robot on different grounds. *Journal of Beijing University of Aeronautics and Astronautics*, **42**(5):984-991 (in Chinese).

Mikalsen, R., Roskilly, A.P., 2007. A review of free-piston engine history and applications. *Applied Thermal Engineering*, **27**(14-15):2339-2352. http://dx.doi.org/10.1016/j.applthermaleng.2007.03.015

Mikalsen, R., Roskilly, A.P., 2009. Coupled dynamic-multidimensional modelling of free-piston engine combustion. *Applied Energy*, **86**(1):89-95. http://dx.doi.org/10.1016/j.apenergy.2008.04.012

Nguyen, Q.V., Park, H.C., 2012. Design and demonstration of a locust-like jumping mechanism for small-scale robots. *Journal of Bionic Engineering*, **9**(3):271-281. http://dx.doi.org/10.1016/S1672-6529(11)60121-2

Powell, O.A., Papas, P., Dreyer, C.B., 2010. Hydrogen-and C1–C3 hydrocarbon-nitrous oxide kinetics in freely propagating and burner-stabilized flames, shock tubes, and flow reactors. *Combustion Science and Technology*, **182**(3):252-283. http://dx.doi.org/10.1080/00102200903357724

Rakopoulos, C.D., Kosmadakis, G.M., Demuynck, J., *et al*., 2011. A combined experimental and numerical study of thermal processes, performance and nitric oxide emissions in a hydrogen-fueled spark-ignition engine. *International Journal of Hydrogen Energy*, **36**(8):5163-5180. http://dx.doi.org/10.1016/j.ijhydene.2011.01.103

Spletzer, B.L., Fisher, G.J., Maritnez, M.A., *et al*., 2001. Hopping Robot. US Patent 6247546.

Stergiopulos, C., Vogt, D., Tolley, M.T., *et al*., 2014. A soft combustion-driven pump for soft robots. ASME Conference on Smart Materials, No. SMASIS2014-7536. http://dx.doi.org/10.1115/SMASIS2014-7536

Tiliakos, N., Tyll, J.S., Herdy, R., *et al*., 2001. Development and testing of a nitrous oxide/propane rocket engine. Joint Propulsion Conference and Exhibit, Paper No. AIAA-2001-3258. https://doi.org/10.2514/6.2001-3258

Tolley, M.T., Shepherd, R.F., Karpelson, M., *et al*., 2014. An untethered jumping soft robot. IEEE/RSJ Intelligent Robots and Systems, p.561-566.

Tsukagoshi, H., Sasaki, M., Kitagawa, A., *et al*., 2005. Design of a higher jumping rescue robot with the optimized pneumatic drive. IEEE International Conference on Robotics and Automation, p.1276-1283.

Wang, H.M., Luan, Y.G., Zhang, K.T., 2012. A Gas Fuel-Powered Hopper. China Patent ZL 201010275632.0 (in Chinese).

Wang, H.M., Luan, Y.G., Oetomo, D., *et al*., 2015. Design, analysis and experimental evaluation of a gas-fuel-powered hopper for robotic actuators. *IEEE/ASME Transactions on Mechatronics*, **20**(5):2264-2275. http://dx.doi.org/10.1109/TMECH.2014.2373354

Willhite, J.A., Yong, C., Barth, E.J., 2013. The high inertance free piston engine compressor—Part II: design and experimental evaluation. *Journal of Dynamic Systems, Measurement, and Control*, **135**(4):041002. http://dx.doi.org/10.1115/1.4023760

Zhao, J., Xu, J., Gao, B., *et al*., 2013. MSU jumper: a single-motor-actuated miniature steerable jumping robot. *IEEE Transactions on Robotics*, **29**(3):602-614. http://dx.doi.org/10.1109/TRO.2013.2249371

中文概要

题　目：燃爆弹跳驱动器仿真与试验研究

目　的：研究燃爆弹跳驱动器热-动力学模型，分析驱动器的输出性能，并通过试验验证驱动器热-动力学模型的正确性。

创新点：1. 建立了燃爆弹跳驱动器热-动力学模型，得到燃爆弹跳驱动器的相关输出参数随时间的变化规律；2. 通过理论仿真与试验测试分析了驱动器的输出性能。

方　法：1. 根据对燃爆弹跳机器人工作过程分析，推导出燃爆弹跳驱动器工作过程中的动力学模型，并对锁紧力与弹簧刚度参数进行测试；2. 根据热-动力学模型推导出燃烧室内压力随时间变化的函数；3. 通过试验测试驱动器驱动弹跳过程中压力和位移随时间的变化曲线，将测试结果与热-动力学模型仿真的结果进行比较。

结　论：1. 建立了燃爆弹跳驱动器的热-动力学模型，得到了驱动器的输出性能参数；2. 试验测试结果与仿真计算结果吻合，证明了驱动器热-动力学模型的正确性。

关键词：热-动力学模型；燃爆驱动器；仿真分析；试验分析；输出性能